




## Article

# A Comprehensive Approach to Facade Design for Preventing Rainwater Penetration: Implementation in Spanish Regions<sup>†</sup>

José M. Pérez-Bella<sup>1,\*</sup>, Javier Domínguez-Hernández<sup>1</sup>, Martín Orna-Carmona<sup>2</sup>, Ángel Salesa-Bordanaba<sup>2</sup> and Scott A. Orr<sup>3</sup>

<sup>1</sup> Department of Construction Engineering, Engineering and Architecture School, University of Zaragoza, María de Luna, s/n, 50018 Zaragoza, Spain; javdom@unizar.es

<sup>2</sup> La Almunia Polytechnic University School, University of Zaragoza, c/ Mayor, 5, 50100 La Almunia de Doña Godina, Spain; morna@unizar.es (M.O.-C.); asalebor@unizar.es (Á.S.-B.)

<sup>3</sup> The Bartlett Faculty of the Built Environment, University College London, 14 Upper Woburn Place, London WC1H 0NN, UK; scott.orr@ucl.ac.uk

\* Correspondence: jmpb@unizar.es

<sup>†</sup> This paper is an extended version of the paper published in Pérez, J.M.; Domínguez, J.; Orr, S.A.; Sanso, L.; Ayensa, A. A comprehensive approach to the performance-based design of facade solutions against rainwater penetration. In Proceedings of the 10th Euro-American Congress of Construction Pathology, Rehabilitation Technology and Heritage Management (REHABEND 2024), Gijón, Spain, 7–10 May 2024; pp. 398–406.

**Abstract:** Rainwater penetration into building facades results in multiple issues, including material and structural degradation, reduced energy efficiency, and health-related concerns among occupants. Currently, the watertightness performance of building facades is assessed based on standardized tests, which simulate generic water supplies and pressure differentials that do not reflect the specific exposure conditions of each facade. Consequently, practitioners' decisions regarding facade design often rely on qualitative and imprecise criteria that do not align with the actual climatic loads. In this article, a comprehensive approach to facade design for preventing rainwater penetration is described, incorporating specific methodological refinements for reliable and practical implementation across various Spanish regions. In this approach, the parameters surpassed during any watertightness test (defined by the magnitude and duration of the water supplies and pressure differentials) are correlated with the recurrence of equivalent climatic exposures at the facade (determined by the climatic conditions of the site, facade height, and surrounding environment), thereby quantitatively characterizing the facade watertightness performance. The findings used to refine this method for implementation in Spain are illustrated and validated using selected case studies, and a comprehensive database is provided to enable its application at 360 locations distributed across various regions of the country.

**Keywords:** rainwater penetration; building facades; standardized tests; climate loads; performance assessment; Spain



**Citation:** Pérez-Bella, J.M.; Domínguez-Hernández, J.; Orna-Carmona, M.; Salesa-Bordanaba, Á.; Orr, S.A. A Comprehensive Approach to Facade Design for Preventing Rainwater Penetration: Implementation in Spanish Regions. *Buildings* **2024**, *14*, 3542. <https://doi.org/10.3390/buildings14113542>

Academic Editors: Ignacio Lombillo, Haydee Blanco, Yosbel Boffill and Alfonso Lozano

Received: 26 September 2024

Revised: 31 October 2024

Accepted: 3 November 2024

Published: 6 November 2024



**Copyright:** © 2024 by the authors. Licensee MDPI, Basel, Switzerland. This article is an open access article distributed under the terms and conditions of the Creative Commons Attribution (CC BY) license (<https://creativecommons.org/licenses/by/4.0/>).

## 1. Introduction

Building facades are complex systems whose design must meet various hygrothermal, aesthetic, construction, acoustic, economic, durability, and fire reaction requirements, among others. Rainwater penetration leads to issues including reduced thermal performance of the thermal envelope, premature deterioration of construction materials, and health risks for building occupants, such as asthma and respiratory symptoms [1–6]. Thus, assessing the watertightness performance of facades is a key factor in predicting their durability, identifying component vulnerabilities, and enhancing potential designs. Wind-driven rain (WDR) occurs when raindrops are deflected by wind action and represent the primary source of water on building facades [3,7]. Combined with simultaneous wind pressure, known as driving rain wind pressure (DRWP), WDR causes rainwater runoff

to surpass the surface tension and capillary pressure thresholds in the pores of facade construction materials, enabling water infiltration. This penetration also occurs directly through sealing defects, fissures, and cracks in the facade surface [8–11].

Over the years, numerous studies have characterized WDR exposure of building facades across various countries, primarily using semi-empirical approaches based on the so-called “WDR relationship” [7,12–16]. Occasionally, the analysis of simultaneous DRWP complemented these characterizations, providing general benchmark indices for comparing exposures among different locations and establishing qualitative design requirements to mitigate rainwater intrusion on building facades [7,17–19]. At the building scale, WDR and DRWP exposures vary significantly based on facade height and geometry, as well as the surrounding terrain, thereby altering the watertightness requirements for facades within the same location [20,21].

However, practitioners’ design decisions are typically based on the performance demonstrated by the facade configurations during standardized watertightness tests, which do not account for this variety of factors. Due to economic and functional constraints, these tests do not simulate the WDR and DRWP exposures expected in each facade being designed. Instead, facade samples are subjected to a constant water supply and incremental pressure differentials, with the duration and generic values of these parameters varying among international test standards [22–27]. Consequently, test parameters are unrelated to the specific environmental conditions expected for each facade, leaving its actual performance in preventing rainwater penetration uncertain. Thus, the traditional WDR and DRWP studies do not adequately inform performance-based facade designs, nor are current design decisions based on quantitative and reliable criteria.

To address this issue, various studies have proposed simulating water supply rates and pressure differentials that correspond to the expected WDR and DRWP exposures linked to a specific design return period, thereby suggesting the adaptation of test parameters and equipment for each facade design [8,28–30]. The return period is a commonly used concept in engineering and risk analyses to estimate the probability of occurrence of a specific event within a given time frame. In other words, it represents the estimated average time between events (climatic, in this case) of a specified magnitude and can be expressed as the inverse of the average frequency of occurrence. For instance, a 10-year return period event has a 10% chance of being exceeded in any given year. However, due to its probabilistic nature, this does not mean that the climatic event will occur exactly once every return period; it may occur once, twice, more, or not at all within that time frame.

From a more realistic and functional perspective, an alternative correlation approach was proposed between the standardized exposure parameters used in testing and actual exposures on any facade (Bayesian performance-based method, also known as the BPB method), thus maintaining the test configurations and allowing for the comparison of results from different tests [31]. This method determines the return period at which a combination of simulated test parameters would occur for any facade characterized by its location, height, and surroundings. Subsequently, this original method was extended to account for the influence of exposure duration during watertightness tests in the calculation of the return period, to include more accurate estimates of the wind profile under unstable atmospheric conditions, and to adjust the WDR value associated with varying predominant raindrop diameters [32,33]. In addition to its enhanced practicality, the BPB method also demonstrated greater ease of calculation compared to previous methods, while maintaining similar accuracy [34].

#### *Bayesian Performance-Based Method*

Considering the particular characteristics of each facade to be designed, the BPB method identifies the recurrence of WDR and DRWP exposures equivalent to those surpassed by the facade configuration during facade watertightness testing (i.e., water spray rate and maximum pressure differential withstood without water leakage) [31–33]. This recurrence, characterized as a return period (in years), constitutes a quantitative and com-

parable measure of the actual watertightness performance of the facade, taking into account the climatic conditions of its location, specific facade features (height and surroundings), and characteristic parameters of the test used for performance approval (where greater magnitude and duration of the endured exposure correspond to higher severity, a longer associated return period, and higher performance).

The BPB calculation defines a system of three equations with three unknowns to determine this return period, allowing for an analytical solution. In the first equation of the system (Equation (1)), the DRWP exposure is estimated using the Bernoulli equation, where  $DRWP_z$  (Pa) represents the driving rain wind pressure at the facade height  $z$  (m) and  $U_{10}$  (m/s) denotes the wind speed records, typically measured using anemometers placed in open areas and at a height ( $z_{data}$ ) of 10 m above ground (this height may be 2 m in agro-climatic weather stations) [35].

To estimate the wind speed at height  $z$  of the facade, the wind profile power law is applied, incorporating the empirical formula proposed by Smedman-Högström and Högström into the Hellmann friction coefficient to better represent the unstable atmospheric conditions associated with WDR events (i.e., characteristic cloud formation mechanisms) [36–38]. This empirical adjustment uses the roughness length of the surrounding terrain  $z_0$  (m), which can be obtained from tabulated values commonly found in the literature [39]. For a conservative and functional calculation, a pressure coefficient of  $C_p = 1$ , constant air density of  $\rho = 1.2 \text{ kg/m}^3$ , and wind direction perpendicular to the facade orientation ( $\cos\theta = 1$ ) can be assumed, thereby simplifying Equation (1). However, other specific coefficients and assumptions may also be used to better represent case studies with particular considerations.

$$DRWP_z \approx C_p \cdot \frac{1}{2} \cdot \rho \cdot (U_{10})^2 \cdot \left( \frac{z}{z_{data}} \right)^{2 \cdot [0.18 + 0.13 \cdot \log z_0 + 0.03 \cdot (\log z_0)^2]} \cdot \cos\theta \quad (1)$$

Traditionally, the WDR calculation ( $\text{L/m}^2$ ) is based on semi-empirical relationships identified since the mid-20th century, which take into account simultaneous records of rainfall  $R_h$  ( $\text{L/m}^2$ ) and wind speed  $U$  (m/s), a driving rain factor (DRF) generalized as  $0.222 \text{ s/m}$ , and the cosine of the angle between the wind direction and that normal to the facade  $\theta$  ( $^\circ$ ) [12,40,41]. Researchers such as Straube and Burnett also incorporate a rain admittance factor (RAF) to weight the exposure at different parts of the facade (Equation (2)) [42].

$$WDR = RAF \cdot DRF \cdot U \cdot R_h \cdot \cos(\theta) \quad (2)$$

In the second equation of the system (Equation (3)), the amount of wind-driven rain  $WDR_z$  ( $\text{L/m}^2$ ) impinged on the facade is determined by adjusting this semi-empirical WDR relationship [43] with a driving rain factor based on the inverse of the terminal falling speed of raindrops [42], and an estimate of the predominant spherical diameter of droplets based on the rainfall record  $R_h$  ( $\text{L/m}^2$ ) [44].  $U_{10}$  (m/s) represents the wind speed records, including the same adjustments and simplifications already mentioned in Equation (1), with  $z_0$  (m) representing the roughness length of the surrounding terrain. To provide a conservative estimate for the most unfavorable area of the facade (typically the uppermost corners of the building), an RAF value of 0.9, the height  $z$  (m) of the facade, and a wind direction perpendicular to the facade orientation can be used again [31,33].

$$WDR_z \approx 1.14 \cdot RAF \cdot \frac{U_{10} \cdot \left( \frac{z}{z_{data}} \right)^{[0.18 + 0.13 \cdot \log z_0 + 0.03 \cdot (\log z_0)^2]}}{-0.16603 \cdot (R_h)^{-1} + 4.92438 \cdot (R_h)^{-0.768} - 0.89002 \cdot (R_h)^{-0.536} + 0.05507 \cdot (R_h)^{-0.304}} \cdot \cos\theta \quad (3)$$

To determine the return period (years) linked to any specific combination of  $WDR_z$  and  $DRWP_z$  exposures (i.e., probability of occurrence), the BPB method includes an innovative approach based on Bayes' theorem (Equation (4)). Since  $DRWP_z$  exposure is solely dependent on the wind speed, the occurrence probability of a specific  $DRWP_z$  value can be

substituted with that of the corresponding wind speed value  $U_{10}$  solved in Equation (1). In turn, the occurrence probability of a particular  $WDR_Z$  exposure, concurrent with the prior wind speed, can be expressed as the occurrence probability of the rainfall value  $R_h$  that can equally be solved in Equation (3). Using this interdependence among variables, the BPB method simplified the mathematical problem into a straightforward probability calculation of two independent variables ( $U_{10}$  and  $R_h$ ), which can be addressed using climatic records collected at each location.

$$\frac{1}{\text{Return period } (WDR_Z \cap DRWP_Z)} = P(WDR_Z \cap DRWP_Z) = P(DRWP_Z) \cdot P(WDR_Z | DRWP_Z) = P(U_{10}) \cdot P(R_h) \quad (4)$$

To calculate the independent probabilities of a specific wind speed value  $P(U_{10})$  and a particular rainfall value  $P(R_h)$ , it is recommended to use an extreme value analysis, such as that defined by the Gumbel distribution [33,45]. This involves statistically analyzing series of annual maxima of  $U_{10}$  and  $R_h$  records at each location: the  $\mu_{(U_{10})}$  and  $\mu_{(R_h)}$  parameters represent the modes of the annual maxima series corresponding to wind speed and rainfall records, respectively, whereas  $\beta_{(U_{10})}$  and  $\beta_{(R_h)}$  denote their dispersion parameters (Equation (5)).

$$\frac{1}{\text{Return period } (WDR_Z \cap DRWP_Z)} \approx \left( 1 - \exp^{-\exp \left( \frac{-(U_{10} - \mu_{(U_{10})})}{\beta_{(U_{10})}} \right)} \right) \cdot \left( 1 - \exp^{-\exp \left( \frac{-(R_h - \mu_{(R_h)})}{\beta_{(R_h)}} \right)} \right) \quad (5)$$

The three-equation system formed by Equations (1), (3) and (5) allows for the calculation of the return period associated with the simultaneous occurrence of any two  $WDR_{Z_i}$  and  $DRWP_{Z_i}$  exposures on the facade being designed, characterized by its location (i.e.,  $\mu_{(U_{10})}$ ,  $\mu_{(R_h)}$ ,  $\beta_{(U_{10})}$ , and  $\beta_{(R_h)}$  parameters) and features (i.e., height  $z$  and surrounding roughness length  $z_0$  values). The resulting equation system offers two distinct possibilities for resolution, depending on the design requirements (Figure 1):

- The first resolution option allows for the quantification of the actual watertightness performance of any facade, expressed as the return period associated with the maximum exposures that the facade configuration withstood during a standardized test. For this purpose, the exposures  $WDR_Z$  ( $L/m^2$ ) and  $DRWP_Z$  (Pa) are set equal to the water supply ( $L/m^2$ ) and pressure differential  $\Delta P$  (Pa) simulated during testing, respectively. The water supply can simply be obtained by multiplying the water spray rate ( $L/m^2 \cdot \text{min}$ ) by the test duration (min). Consequently, only the return period linked to both exposures and the intermediate wind speed  $U_{10}$  and rainfall  $R_h$  values remain as unknowns to be solved in the three-equation system.
- Alternatively, it is also possible to quantify the pressure differential  $\Delta P$  (i.e.,  $DRWP_Z$  exposure) that the facade configuration must withstand during any given test to approve a required watertightness performance (i.e., a return period established by future regulatory requirements or design criteria). Setting longer return periods leads to withstanding higher pressure differentials, thus requiring facade designs of higher watertightness performance. In this resolution option, the wind speed  $U_{10}$  and rainfall  $R_h$  values can be determined directly based on the water spray rate and duration specified in the selected test ( $WDR_Z$  exposure) and required return period, using the two-equation system formed by Equations (3) and (5). Subsequently, the sought  $\Delta P$  value can be solved using Equation (1).

Setting other pairs of unknowns lacks physical meaning, as  $U_{10}$  and  $R_h$  variables are merely intermediate variables, whereas the duration and water spray rate (i.e.,  $WDR_Z$  exposure) are standardized constants predetermined for each watertightness test.

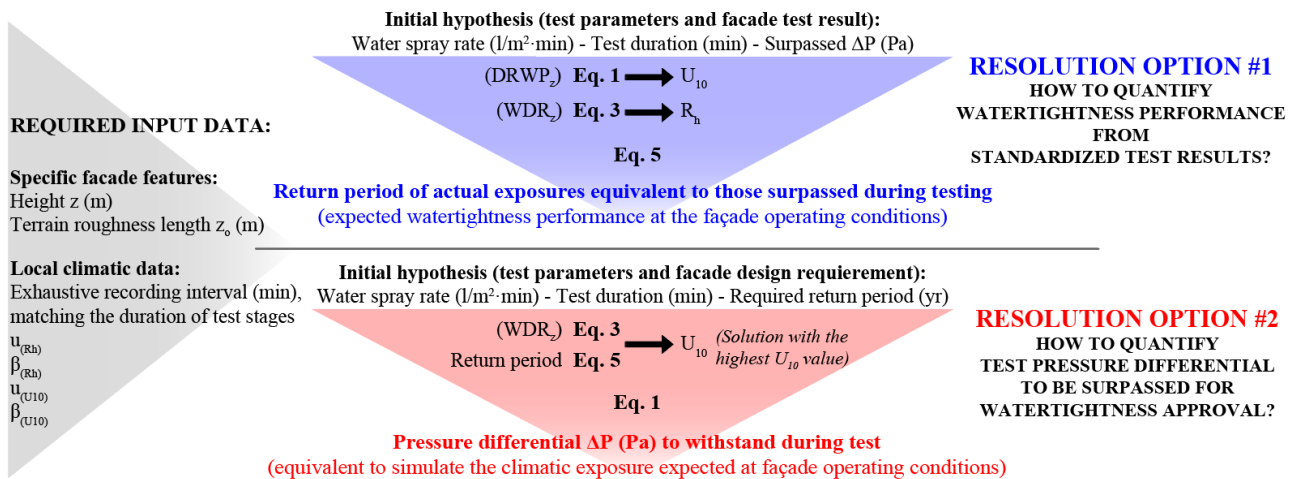


**Figure 1.** Flowchart of the resolution options using the original BPB method.

This article is a revised and expanded version of a paper entitled A comprehensive approach to the performance-based design of façade solutions against rainwater penetration, which was presented at REHABEND 2024 Congress, Gijón, Spain (7–10 May 2024) [46]. The article provides a comprehensive database that enables the implementation of the BPB method at 360 locations distributed across various Spanish regions. Additionally, some methodological uncertainties that impact the reliability of the BPB method and limit its practicality are addressed in this implementation:

- By re-analyzing weather records to exclude wind speed records that are not concurrent with rainfall, improved mode and dispersion parameters related to wind speed can be determined, thereby enhancing the physical consistency of the formulation.
- By identifying general regressions that allow for the application of the method in any location using any sub-daily weather records with minimal calculation effort, the dependency on available wind speed records associated with exhaustive recording intervals can be overcome.

The proposed methodological refinements and database calculation parameters are discussed and validated through two selected case studies located in the cities of Málaga (Andalusia), Pontevedra (Galicia), and San Javier (Murcia), which provide a clear contrast in facade operating conditions.

## 2. Materials and Methods

The primary limitation to the extensive implementation of the BPB method in facade design lies in the requirement for raw climatic data linked to exhaustive recording intervals. Thus, the mode and dispersion parameters  $\mu_{(U_{10})}$ ,  $\mu_{(R_h)}$ ,  $\beta_{(U_{10})}$ , and  $\beta_{(R_h)}$  used in Equation (5) are related to the recording interval of the available weather data at each location (e.g., hourly or daily records). In contrast, the wind speed  $U_{10}$  and rainfall  $R_h$  values solved in Equations (1) and (3) are related to the duration specified in each watertightness test, which typically ranges from 5 to 15 min for differential pressure stages [22–27]. When the test duration does not align with the available recording interval at the location, misleading results that do not reliably represent the recurrence of simultaneous  $WDR_z$  and  $DRWP_z$  exposures may be obtained: an exposure intensity sustained over a longer time interval represents a less frequent and more challenging exposure compared with the same intensity applied for a shorter duration. Therefore, the availability of exhaustive weather records can be a limiting factor for reliably using the method in certain locations.

In turn, it is crucial to ensure that the wind speed values  $U_{10}$  used in the equation system specifically refer to wind speed records concurrent with rainfall, in order to maintain the physical sense of the calculation. Using unscreened wind speed records that do not



account for their co-occurrence with rainfall may also lead to unreliably watertightness performance [31–33].

To reliably implement the BPB method in Spain and reduce its dependence on exhaustive weather data and calculation effort, (1) a preliminary re-analysis of available climatic records was performed, and (2) an intermediate calculation was included to extrapolate equivalent  $U_{10}$  and  $R_h$  variables matching the available recording interval at each location:

Firstly (1), simultaneous wind speed and rainfall data recorded at intervals of 10, 30, or 60 min (depending on the region) over a 10-year period were analyzed at 360 Spanish locations, thus minimizing biases due to the occurrence of atypical climatic years. At each site, screened series of wind speed records simultaneous with rainfall  $U_{10SIM}$  (m/s) were identified, thus discarding those wind data irrelevant to the assessment of rainwater penetration exposure on facades. Subsequently, the maximum annual values of these screened series were identified, allowing for a more reliable determination of the mode and dispersion parameters for use in Equation (5) (Table 1). In this way, both resulting parameters  $\mu_{(U_{10SIM})}$  and  $\beta_{(U_{10SIM})}$  ensure the physical sense of the equation system, allowing for the estimation of return periods that actually represents the recurrence of  $DRWP_Z$  exposures.

**Table 1.** Calculation of the mode and dispersion parameters from the maximum annual records of the analyzed variable.

Symbol	Formula	Description
$x_i$	-	Maximum annual records of the variable, associated with a specific recording interval.
$N$	-	Number of input data $x_i$ of the variable (number of years with maximum annual records).
$x_{avg}$	$= \frac{\sum x_i}{N}$	Data average of the annual maxima.
$\sigma_x$	$= \sqrt{\frac{\sum (x_i - x_{avg})^2}{N}}$	Standard deviation of the annual maxima.
$y_i$	$= -\ln\left(\ln\left(\frac{N+1}{i}\right)\right)$	$N$ values of the reduced variable $y$ , ranging $i$ from 1 to $N$ .
$y_{avg}$	$= \frac{\sum y_i}{N}$	Data average of the $N$ values of the reduced variable $y_i$ .
$\sigma_y$	$= \sqrt{\frac{\sum (y_i - y_{avg})^2}{N}}$	Standard deviation of the $N$ values of the reduced variable $y_i$ .
$\mu$	$= x_{avg} - y_{avg} \frac{\sigma_x}{\sigma_y}$	Mode of the variable (Equation (5)), linked to the specific recording interval.
$\beta$	$= \frac{\sigma_x}{\sigma_y}$	Dispersion parameter of the variable (Equation (5)), linked to the specific recording interval.

Secondly (2), to ensure the mathematical consistency of Equation (5), the  $U_{10SIM}$  and  $R_h$  values solved in Equations (1) and (3) (associated with the duration of the pressure stages established in watertightness tests) must be extrapolated to the recording interval characterizing the available mode and dispersion parameters ( $\mu$  and  $\beta$ ) at the location (Figure 2). For this purpose, a recent study that proposed general forms of regressions to extrapolate extreme values of rainfall intensity (mm/min) and wind speed (m/s) across different sub-daily recording intervals may be considered [47].

For rainfall intensity, a power-type regression was proposed to relate the maximum annual records associated with different sub-daily intervals (Equation (6)).  $R_{h(t)}$  (mm/min) represents the rainfall intensity associated with any  $t$ -minute recording interval during extreme precipitation events, whereas the empirical coefficients  $a$  and  $b$  are site-dependent.

$$R_{h(t)} = a \cdot t^{-b} \quad (6)$$

Similarly, a logarithmic-type regression was found to be the most suitable for relating the maximum annual wind speeds linked to different sub-daily intervals (Equation (7)). In this case,  $U_{10(t)}$  (m/s) represents the wind speed associated with a  $t$ -minute record of extreme wind events. The empirical coefficients  $c$  and  $d$  also vary according to the location.

$$U_{10(t)} = -c \cdot \ln(t) + d \quad (7)$$

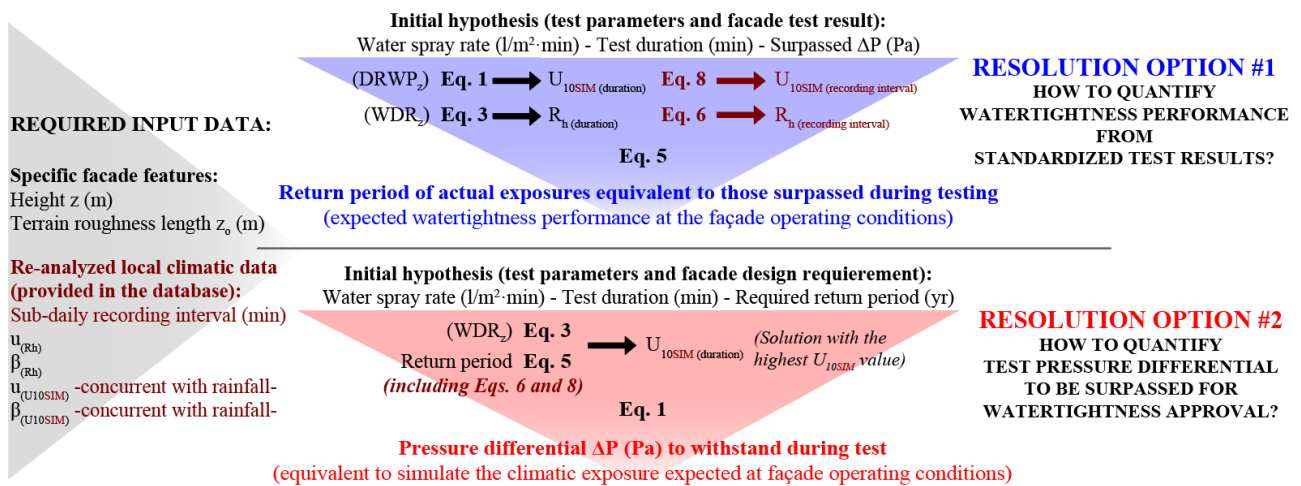


**Figure 2.** Methodological refinements incorporated into the implementation of the BPB method in Spain, including the re-analysis of wind speed records concurrent with rainfall and an intermediate cross-multiplication to extrapolate calculation variables linked to the recording interval required in Equation (5).

However, no distinction was made between extreme wind records concurrent and non-concurrent with rainfall in the validation of the aforementioned equation. Therefore, the suitability of this type of logarithmic regression for wind speed values concurrent with rainfall  $U_{10SIM}$  (i.e., using tailored  $c_{SIM}$  and  $d_{SIM}$  coefficients) remains undefined (Equation (8)).

$$U_{10SIM(t)} = -c_{SIM} \cdot \ln(t) + d_{SIM} \quad (8)$$

In this study, the available records at the 360 analyzed Spanish locations were also summed or averaged to produce aggregate data series for different recording intervals (e.g., generating 60, 120, 180, 360, 480, 720, and 1440 min data series of rainfall and wind speed from the available 30 min records). For this purpose, the sum and average procedures established by the World Meteorological Organization were applied to obtain rainfall and wind speed aggregated values, respectively [35]. To minimize uncertainties, where a record was missing (due to maintenance periods, breakdowns, data storage issues, or other factors), all aggregate data associated with that record were also disregarded (e.g., the 120, 180, 360 min data, etc., that included a missing hourly record).

In turn, the annual maximum records linked to each aggregate series were obtained and subsequently averaged, in order to obtain a representative maximum per recording interval, variable (rainfall intensity and wind speed), and location. By conducting a least-squares regression (LSR) analysis on these average maxima, site-specific coefficients for Equations (6) and (7) were identified (i.e., coefficients  $a$ ,  $b$ ,  $c$ , and  $d$ ). The calculations required for the implementation of this LSR analysis, as well as for producing each aggregated data series, were automated using commonly available spreadsheet programs [48]. Repeating the same procedure, the coefficients  $c_{SIM}$  and  $d_{SIM}$  applicable at each location were also identified by using aggregated data series produced from wind speed records only concurrent with rainfall.

Although multiple recording intervals were aggregated to improve the accuracy of the LSR analysis, it could also be applied using weather records related to just two sub-daily recording intervals (e.g., by aggregating daily records), thereby significantly reducing the computational effort of the required re-analysis. Similarly, in countries where the availability of sub-daily data collected at the stations may pose a challenge, weather databases derived from models and reanalyzes, such as those provided by the European Centre for Medium-Range Weather Forecasts on a  $0.25^\circ \times 0.25^\circ$  grid for Europe, could be used while acknowledging the inherent uncertainties of these models [49].

The correlation results obtained concerning these regressions across different Spanish regions are presented in Section 3, as well as the mode and dispersion parameters for  $U_{10}$ ,  $U_{10SIM}$ , and  $R_h$  identified at each location, thus enabling a practical and reliable implementation of the BPB method in most of Spain. In turn, Section 4 discusses and validates these methodological refinements through their application in two facade case studies concerning three Spanish cities.

#### Scope of the Conducted Implementation

To address the re-analysis of wind speed records and to identify regressions that allow for the extrapolation of equivalent wind and rainfall extremes across sub-daily recording intervals, exhaustive climatic records were analyzed from 360 weather stations distributed across 10 Spanish regions (Figure 3). These regions are representative of the broad climatic variability of the country, ranging from oceanic to hot arid climates (Cfb and BWh climates, respectively, according to the Köppen–Geiger classification) [50,51]. In any case, most of the analyzed territory features Mediterranean climates (hot-summer and warm-summer subtypes; Csa and Csb, respectively) or cold semi-arid climates (BSk).



**Figure 3.** Coverage distribution of the Spanish territory addressed in this study for the application of the BPB method, including the locations of the case studies presented in Section 4. Source: Own elaboration based on climatic graphic data available in [51].



Due to this climatic variability, the mean annual rainfall notably varies among the analyzed locations, ranging from less than 200 mm/yr at eight sites in the Region of Murcia, southeastern Andalusia, and southern Castile and León, to more than 2500 mm/yr in Fornelos de Montes (a coastal location in southwestern Galicia). Spain is also characterized by rugged topography, allowing for the analysis of locations at both sea level and high altitudes, such as Xares (Galicia), at 1762 m. This rugged topography also affects the predominant winds across different regions, resulting in significant variations between coastal areas, characterized by high mean wind speeds, and inland zones such as northeastern Andalusia, where mean wind speeds barely reach 0.5 m/s for a 30 min recording interval (e.g., Villacarrillo and Santo Tomé Stations).

The climatic data analyzed were obtained from official repositories provided by regional meteorological or agro-climatic agencies, such as those of Galicia, Andalusia, Basque Country, La Rioja, and Castile and León [52–56], as well as national agencies [57,58]. Most Spanish regions not covered in this study, shaded in grey in Figure 3, either lack publicly accessible repositories or require substantial fees for access through the Spanish Meteorological Agency.

All the selected data correspond to uninterrupted 10-year series, spanning from 2008 to 2022, depending on the region. These data refer to 10, 30, and 60 min recording intervals, based on the available source at each region (see Table 2). The age and quality of these records (on average, only 0.29% of data are missing, with a maximum of 10.5% in Cartagena, Murcia) ensure the representativeness of the results and minimize deviations due to extended data gaps. Although the years analyzed in each region slightly differ, the identified calculation parameters always stem from averaging the extreme values recorded annually over the 10-year analysis period, thereby ensuring that the influence of any climatologically atypical year is diluted within the overall dataset. Furthermore, the period from 2008 to 2022 is not sufficiently long to demonstrate significant climatic variations due to climate change, and in any case, a minimum of five years (2013–2017) is shared among all stations.

**Table 2.** Distribution of the 360 analyzed stations across Spain and characteristics of the consulted climatic data.

Region	# of Locations	$z_{data}$ (m)	Recording Interval (min)	Years Considered [Source]
Andalusia (87,597 km <sup>2</sup> ; 8.4 M inhabitants)	85	2	30	2011–2020 [53]
Aragon (47,719 km <sup>2</sup> ; 1.3 M inhabitants)	27	2	60	2013–2022 [58]
Balearic Islands (4992 km <sup>2</sup> ; 1.2 M inhabitants)	9	2	60	2013–2022 [58]
Basque Country (7234 km <sup>2</sup> ; 2.2 M inhabitants)	19	10	10	2009–2018 [54]
Castile and León (94,222 km <sup>2</sup> ; 2.4 M inhabitants)	52	2	30	2011–2020 [56]
Castile–La Mancha (79,463 km <sup>2</sup> ; 2.1 M inhabitants)	39	2	60	2013–2022 [58]
Galicia (29,575 km <sup>2</sup> ; 2.7 M inhabitants)	40	10	10	2008–2017 [52]
La Rioja (5045 km <sup>2</sup> ; 0.3 M inhabitants)	21	2	60	2010–2019 [55]
Murcia (11,313 km <sup>2</sup> ; 1.6 M inhabitants)	41	2	60	2011–2020 [57]
Navarre (10,391 km <sup>2</sup> ; 0.7 M inhabitants)	27	2	60	2013–2022 [58]

### 3. Results

For locations with available 10 min records, eight additional series were generated: 20, 30, 40, 60, 360, 480, and 720 min records and daily records. In regions with 30 min records, the additional series encompassed 60, 120, 180, 360, 480, 720, and 1440 min data. Where hourly data were available, additional series covering 360, 480, 720, and 1440 min recording intervals were produced. The annual maxima were identified and averaged to determine a single representative value of rainfall intensity, wind speed, and wind speed concurrent with precipitation, associated with each recording interval at the 360 locations.

The results obtained from applying an LSR analysis to these average maxima (i.e.,  $a$ ,  $b$ ,  $c$ ,  $d$ ,  $c_{SIM}$ , and  $d_{SIM}$  coefficients) are tabulated and provided in a comprehensive database that enables the implementation of the method in the analyzed regions (see Supplementary Material). This database also presents the mode ( $\mu$ ) and dispersion ( $\beta$ ) parameters for each variable, corresponding to the most exhaustive recording interval available at each location. This allows for minimizing the uncertainty in the extrapolations defined by Equations (6)–(8), since this interval is typically close to the duration of standardized watertightness tests.

This database also includes information on the altitude and geographical coordinates of each location, missing data, and average annual rainfall and wind speed, as well as the mean annual maxima identified for each variable (rainfall, wind speed, and wind speed concurrent with rainfall) for each aggregated sub-daily interval.

As can be observed in this database, the general forms of regression presented in Section 2 can be reliably used at Spanish locations, even for extrapolating annual maximum wind speeds concurrent with rainfall among different sub-daily recording intervals. The power-type regression for rainfall intensity (Equation (6)) achieves a mean coefficient of determination  $R^2$  of 0.993, with a minimum correlation of 0.925 in the city of Lorca (Murcia). These coefficients of determination remain consistent regardless of the available recording interval: for locations with 10 min rainfall records, the mean  $R^2$  value reaches 0.997, while it is 0.996 for sites with 30 min data and 0.991 for those with hourly records. This confirms the reliability of the regression across recording intervals from as short as 10 min to daily.

The average  $R^2$  value slightly decreases to 0.958 for the correlations in Equation (7). However, this logarithmic-type regression demonstrates even greater reliability for extrapolating annual maximum wind speeds concurrent with rainfall (Equation (8)), with an average  $R^2$  value of 0.982, ranging from 1.000 (Rincón de Soto, La Rioja; Herencia and Armuña de Tajuña, both in Castile–La Mancha) to 0.755 (Málaga, Andalusia). In this case, the mean  $R^2$  value reaches 0.977 for locations with 10 min wind speed data, 0.980 for those where 30 min records are available, and 0.986 for sites with hourly records. There are also no significant differences between locations that include 3 s records (wind gust intervals), with a mean  $R^2$  equal to 0.980, and those without these data (0.983), thus demonstrating the consistency of the regression even for time resolutions significantly shorter than the typical durations used in the pressure stages of watertightness tests.

Consequently, both Equations (6) and (8) can be used alongside the BPB method to reliably extrapolate, via an intermediate cross-multiplication step, those extreme wind speed  $U_{10SIM}$  and rainfall  $R_h$  values linked to the recording interval required by the mode and dispersion parameters available in Equation (5).

### 4. Discussion

Three Spanish cities (see Figure 3), representing different climates and available recording intervals, were selected for validation: Málaga Station (Andalusia, #64 in the Supplementary Material), with a hot-summer Mediterranean climate and 30 min agro-climatic records measured at a height of 2 m ( $z_{data} = 2$  m); Pontevedra (Lourizán Station, Galicia, #265), with available 10 min weather records of rainfall and wind speed and a temperate oceanic climate; and San Javier (Santiago de la Ribera Station, Region of Murcia, #329), with hourly agro-climatic data and a cold semi-arid climate. Across the 10 years analyzed at

each location, the missing data ranged from 0.095% in Málaga and 0.009% in Pontevedra to 10.096% in San Javier.

For improved readability, the calculation parameters characteristic of the three locations, based on the re-analysis and aggregated data series produced for different recording intervals, have been extracted from the database and are summarized in Table 3.

**Table 3.** Summary of the calculation parameters applicable in the three selected cities for the case studies.

<b>Málaga Station (#64). Andalusia</b>											
Maximum rainfall intensity (mm/min); average of 10 annual maxima for each recording interval											
	30'	40'	hourly	120'	180'	360'	480'	720'	daily	Equation (6) (by LSR; $R^2 = 0.999$ )	
	0.677		0.425	0.253	0.158	0.123	0.095	0.074	0.041	$R_h(t) = 7.933 \cdot t^{-0.716}$	
$\mu_{(Rh)} =$	12.102								a =	7.933	
$\beta_{(Rh)} =$	16.596								b =	0.716	
Maximum wind speed (m/s); average of 10 annual maxima for each recording interval											
gust	30'	40'	hourly	120'	180'	360'	480'	720'	daily	Equation (7) (by LSR; $R^2 = 0.985$ )	
	6.847		6.181	5.716	5.181	4.883	4.727	4.091	3.349	$U_{10(t)} = -0.861 \cdot \ln(t) + 9.822$	
$\mu_{(U10)} =$	6.284								c =	0.861	
$\beta_{(U10)} =$	1.138								d =	9.822	
Maximum wind speed concurrent with rainfall (m/s); average of 10 annual maxima for each recording interval											
gust	30'	40'	hourly	120'	180'	360'	480'	720'	daily	Equation (8) (by LSR; $R^2 = 0.986$ )	
	5.272		4.479	3.734	2.848	2.197	2.125	1.531	1.039	$U_{10SIM(t)} = -1.127 \cdot \ln(t) + 9.013$	
$\mu_{(U10SIM)} =$	4.687								c <sub>SIM</sub> =	1.127	
$\beta_{(U10SIM)} =$	1.181								d <sub>SIM</sub> =	9.013	
<b>Pontevedra (Lourizán Station; #265). Galicia</b>											
Maximum rainfall intensity (mm/min); average of 10 annual maxima for each recording interval											
	10'	20'	30'	40'	hourly	360'	480'	720'	daily	Equation (6) (by LSR; $R^2 = 0.999$ )	
	1.064	0.640	0.505	0.404	0.326	0.114	0.092	0.072	0.047	$R_h(t) = 4.138 \cdot t^{-0.617}$	
$\mu_{(Rh)} =$	6.363								a =	4.138	
$\beta_{(Rh)} =$	8.637								b =	0.617	
Maximum wind speed (m/s); average of 10 annual maxima for each recording interval											
gust	10'	20'	30'	40'	hourly	360'	480'	720'	daily	Equation (7) (by LSR; $R^2 = 0.953$ )	
	21.963	10.169	9.489	9.012	8.723	8.216	6.359	6.117	5.555	4.568	$U_{10(t)} = -1.619 \cdot \ln(t) + 15.398$
$\mu_{(U10)} =$	9.226								c =	1.619	
$\beta_{(U10)} =$	1.905								d =	15.398	
Maximum wind speed concurrent with rainfall (m/s); average of 10 annual maxima for each recording interval											
gust	10'	20'	30'	40'	hourly	360'	480'	720'	daily	Equation (8) (by LSR; $R^2 = 0.970$ )	
	21.746	9.824	9.068	8.212	7.517	7.098	5.223	4.642	4.015	3.091	$U_{10SIM(t)} = -1.765 \cdot \ln(t) + 14.997$
$\mu_{(U10SIM)} =$	8.975								c <sub>SIM</sub> =	1.765	
$\beta_{(U10SIM)} =$	1.715								d <sub>SIM</sub> =	14.997	

Table 3. Cont.

San Javier (Santiago de la Ribera Station; #329). Region of Murcia								
Maximum rainfall intensity (mm/min); average of 10 annual maxima for each recording interval								
	hourly	120'	180'	360'	480'	720'	daily	Equation (6) (by LSR; $R^2 = 0.978$ )
	0.479	0.300	0.236	0.129	0.118	0.079	0.048	$R_h(t) = 10.463 \cdot t^{-0.734}$
$\mu_{(Rh)} =$	15.374						a =	10.463
$\beta_{(Rh)} =$	27.030						b =	0.734
Maximum wind speed (m/s); average of 10 annual maxima for each recording interval								
gust	hourly	120'	180'	360'	480'	720'	daily	Equation (7) (by LSR; $R^2 = 0.982$ )
13.226	5.855	5.511	5.339	5.106	4.974	4.716	3.942	$U_{10(t)} = -0.897 \cdot \ln(t) + 10.265$
$\mu_{(U10)} =$	4.786						c =	0.897
$\beta_{(U10)} =$	2.160						d =	10.265
Maximum wind speed concurrent with rainfall (m/s); average of 10 annual maxima for each recording interval								
gust	hourly	120'	180'	360'	480'	720'	daily	Equation (8) (by LSR; $R^2 = 0.997$ )
11.880	5.179	4.769	4.146	3.345	3.028	2.572	1.804	$U_{10SIM(t)} = -0.971 \cdot \ln(t) + 9.081$
$\mu_{(U10SIM)} =$	4.001						$c_{SIM} =$	0.971
$\beta_{(U10SIM)} =$	2.379						$d_{SIM} =$	9.081

By comparing extreme averages related to the same recording interval (e.g., hourly data), it can be observed that San Javier presents the highest rainfall intensity (0.479 mm/min), despite its much lower annual rainfall compared to Pontevedra (270 vs. 1514 mm/yr). Unlike Pontevedra, where rainfall events are distributed throughout the year, Málaga and San Javier experience transient but intense precipitations, such as those caused by the cold drop (isolated depressions at high levels), which can potentially be more unfavorable when considering the risk of rainwater penetration in building facades [59].

On the other hand, when comparing the hourly extreme winds (both unscreened and concurrent with rainfall), Pontevedra shows the highest values, although it should be noted that these data were recorded at a greater anemometer height. Therefore, without a quantitative and comprehensive method like the one presented, it would be difficult to intuit which location presents the most unfavorable combined exposures. Similarly, any approach based solely on average annual rainfall or wind speed could lead to inadequate or unreliable design perceptions, as demonstrated below.

In turn, two facade designs have been considered in each location (referred to as cases A and B for conciseness and clarity), allowing for the application of both resolution options established by the BPB method:

- In case A, the building facade to be designed has a height  $z = 9$  m (single-family dwelling) and is located on the outskirts of each city (roughness length  $z_0 = 1.5$  m) [39]. The objective is to quantify the actual watertightness performance of the facade configuration under consideration, which is able to withstand a pressure differential of 150 Pa during the EN 12865 watertightness test. This test is characterized by pressure stages of 10 min and a water spray rate of  $2 \text{ L/m}^2 \cdot \text{min}$  [22].
- In case B, the objective is to approve a 36 m high curtain wall ( $z = 36$  m) that will ensure 100 years of watertightness performance in each city center (roughness length  $z_0 = 3.0$  m) [39]. The pressure differential  $\Delta P$  that the facade configuration under consideration must withstand during the EN 12155 test (characterized by 5 min pressure stages and a water spray rate of  $2 \text{ L/m}^2 \cdot \text{min}$ ) should be determined [23].



#### 4.1. Case A: Quantifying the Watertightness Performance of the Facade Configuration

The watertightness performance of the facade configuration under consideration will vary depending on the local climatic conditions, as presented below.

##### 4.1.1. Málaga

The wind speed concurrent with rainfall required to generate a DRWP<sub>z</sub> exposure of 150 Pa on the facade can be obtained by solving Equation (1), considering that the available 30 min wind speed records refer to a measurement height of 2 m (agro-climatic data).

$$150 \text{ Pa} = 1 \cdot \frac{1}{2} \cdot 1.2 \cdot \left( U_{10SIM(10min)} \right)^2 \cdot \left( \frac{9}{2} \right)^{2 \cdot [0.18 + 0.13 \cdot \log 1.5 + 0.03 \cdot (\log 1.5)^2]} \cdot 1 \Rightarrow U_{10SIM(10min)} = 11.637 \text{ m/s}$$

In turn, the rainfall intensity required to provide 20 mm of wind-driven rain WDR on this facade (equivalent to 2 L/m<sup>2</sup>·min within a 10 min period), while there is a concurrent wind speed of 11.637 m/s, can be obtained using Equation (3):

$$20 \text{ mm} = 1.14 \cdot 0.9 \cdot \frac{11.637 \cdot \left( \frac{9}{2} \right)^{[0.18 + 0.13 \cdot \log 1.5 + 0.03 \cdot (\log 1.5)^2]}}{-0.16603 \cdot \left( R_{h(10min)} \right)^{-1} + 4.92438 \cdot \left( R_{h(10min)} \right)^{-0.768} - 0.89002 \cdot \left( R_{h(10min)} \right)^{-0.536} + 0.05507 \cdot \left( R_{h(10min)} \right)^{-0.304}}$$

$$R_{h(10min)} = 6.865 \text{ mm} = 0.686 \text{ mm/min}$$

As the duration of the pressure stages of the EN 12865 test (10 min) does not match the recording interval available at Málaga, it is necessary to apply the intermediate cross-multiplication based on Equations (6) and (8), thus extrapolating the 30 min values equivalent to the solved rainfall  $R_h$  and wind speed  $U_{10SIM}$  values:

$$R_{h(30min)} = R_{h(10min)} \cdot \frac{7.933 \cdot 30^{-0.716}}{7.933 \cdot 10^{-0.716}} = 0.313 \text{ mm/min} = 9.39 \text{ mm}$$

$$U_{10SIM(30min)} = U_{10SIM(10min)} \cdot \frac{-1.127 \cdot \ln(30) + 9.013}{-1.127 \cdot \ln(10) + 9.013} = 9.392 \text{ m/s}$$

Both 30 min equivalent values can be applied in Equation (5) to calculate the return period associated with the maximum exposure that this facade configuration withstood during the test (78.3 years).

$$\frac{1}{\text{Return period (20 mm} \cap \text{150 Pa)}} = \left( 1 - \exp^{-\exp \left( \frac{-9.392 - 4.687}{1.181} \right)} \right) \cdot \left( 1 - \exp^{-\exp \left( \frac{-9.39 - 12.102}{16.596} \right)} \right)$$

$$\text{Return period (20 mm} \cap \text{150 Pa)} = 78.3 \text{ years}$$

##### 4.1.2. Pontevedra

The same previous calculation is now replicated for Pontevedra, where the mode and dispersion parameters corresponding to the available 10 min rainfall and wind speed records refer to a measurement height of 10 m. As this recording interval matches the duration of the test pressure stages, it is not required to use Equations (6) and (8). Thus, the rainfall  $R_h$  and wind speed  $U_{10SIM}$  values obtained from Equations (1) and (3) can be directly applied in Equation (5), resulting in a return period of 108.5 years.

This demonstrates that the extreme climatic exposures surpassed during the EN 12865 watertightness test can occur with slightly greater frequency in Málaga compared to Pontevedra. In other words, the facade configuration under consideration offers worse watertightness performance in Málaga, for the same design features.

#### 4.1.3. San Javier

In the case of San Javier, the calculation parameters related to the available hourly recording interval of agro-climatic data also require applying the intermediate cross-multiplication to extrapolate hourly rainfall  $R_h$  and wind speed  $U_{10SIM}$  values that can be used in Equation (5). By applying the coefficients  $a$ ,  $b$ ,  $c_{SIM}$ , and  $d_{SIM}$  corresponding to San Javier, it is also possible to extrapolate hourly extreme values of rainfall  $R_{h(60 \text{ min})}$  and wind speed concurrent with rainfall  $U_{10SIM(60 \text{ min})}$ , based on their equivalents associated with the 10 min test duration. Thus, from the  $R_{h(10 \text{ min})}$  value equal to 6.865 mm, an equivalent extreme  $R_{h(60 \text{ min})}$  value of 11.04 mm is obtained. Similarly, from the  $U_{10SIM(10 \text{ min})}$  value equal to 11.637 m/s, an extreme equivalent  $U_{10SIM(60 \text{ min})}$  value of 8.679 m/s can be obtained.

By using both hourly values along with the mode and dispersion parameters characteristic of the site in Equation (5), a lower watertightness performance is identified compared to the other locations (11.1 years), due to the unfavorable climate at the site. Thus, for instance, the result obtained would suggest using a different facade configuration able to provide a higher watertightness performance in the city of San Javier.

#### 4.2. Case B: Determining the Pressure Differential to Withstand in Any Watertightness Test

The pressure differential  $\Delta P$  that a facade configuration must withstand during a watertightness test to approve a required performance will vary depending on the local climatic conditions and the test parameters. For this case study (a 36 m curtain wall in an urban center) and considering the EN 12155 test, the calculation for the second resolution option is presented below.

##### 4.2.1. Málaga

First, the wind speed  $U_{10SIM}$  and rainfall  $R_h$  values associated with the required 100-year recurrence must be identified by solving the two-equation system defined by Equations (3) and (5). In this case, it is also necessary to apply the intermediate cross-multiplication that allows for extrapolating the 30 min values (recording interval at the location) equivalent to those associated with the 5 min duration of the test, in order to maintain the mathematical consistency of Equation (5):

$$R_{h(30 \text{ min})} = R_{h(5 \text{ min})} \cdot \frac{7.933 \cdot 30^{-0.716}}{7.933 \cdot 5^{-0.716}} = 0.277 \cdot R_{h(5 \text{ min})}$$

$$U_{10SIM(30 \text{ min})} = U_{10SIM(5 \text{ min})} \cdot \frac{-1.127 \cdot \ln(30) + 9.013}{-1.127 \cdot \ln(5) + 9.013} = 0.720 \cdot U_{10SIM(5 \text{ min})}$$

$$10 \text{ mm} = 1.14 \cdot 0.9 \cdot \frac{U_{10SIM(5 \text{ min})} \cdot \left(\frac{36}{2}\right)^{[0.18+0.13 \cdot \log 3.0+0.03 \cdot (\log 3.0)^2]}}{-0.16603 \cdot (R_{h(5 \text{ min})})^{-1} + 4.92438 \cdot (R_{h(5 \text{ min})})^{-0.768} - 0.89002 \cdot (R_{h(5 \text{ min})})^{-0.536} + 0.05507 \cdot (R_{h(5 \text{ min})})^{-0.304}}$$

$$\frac{1}{100 \text{ years}} = \left( 1 - \exp^{-\exp \left( \frac{-(0.720 \cdot U_{10SIM(5 \text{ min})} - 4.687)}{1.181} \right)} \right) \cdot \left( 1 - \exp^{-\exp \left( \frac{-(0.277 \cdot R_{h(5 \text{ min})} \cdot 30 - 12.102)}{16.596} \right)} \right)$$

$$U_{10SIM(5 \text{ min})} = 13.275 \text{ m/s} \quad R_{h(5 \text{ min})} = 1.522 \text{ mm} = 0.304 \text{ mm/min}$$

Although two possible combinations of variables are linked to a 100-year recurrence (max.  $R_h$ –min.  $U_{10SIM}$  and min.  $R_h$ –max.  $U_{10SIM}$ ), only the second combination is of interest, as it determines the most unfavorable pressure differential (i.e., maximum wind speed result) to be surpassed during the trial (the discarded combination was  $U_{10SIM(5 \text{ min})} = 2.668 \text{ m/s}$  and  $R_{h(5 \text{ min})} = 10.634 \text{ mm}$ ). Thus, the obtained wind speed concurrent with rainfall directly allows for determining the  $\Delta P$  value that must be surpassed by the curtain wall under consideration during the EN 12155 test (Equation (1)):

$$DRWP = \Delta P = 1 \cdot \frac{1}{2} \cdot 1.2 \cdot \left( U_{10SIM(5 \text{ min})} \right)^2 \cdot \left( \frac{36}{2} \right)^{2 \cdot [0.18 + 0.13 \cdot \log 3.0 + 0.03 \cdot (\log 3.0)^2]} \cdot 1 = 446 \text{ Pa}$$

#### 4.2.2. Pontevedra

The same previous calculation is now applied in Pontevedra by considering a  $z_{\text{data}}$  equal to 10 m, the mode and dispersion parameters corresponding to the available 10 min records, and the site-specific coefficients  $a$ ,  $b$ ,  $c_{SIM}$ , and  $d_{SIM}$  (Table 3). In this case, the required  $\Delta P$  value reaches 329 Pa (with a wind speed concurrent with rainfall  $U_{10SIM(5 \text{ min})}$  of 17.025 m/s and a rainfall value  $R_{h(5 \text{ min})}$  of 1.834 mm), suggesting that a lower watertightness performance than in Málaga must be demonstrated in this test to approve the design requirements.

#### 4.2.3. San Javier

When applying the same calculation in the city of San Javier (using hourly agro-climatic data), the  $\Delta P$  value to be surpassed during the test increases to 1102 Pa for this 100-year watertightness performance, with  $U_{10SIM(5 \text{ min})} = 20.879$  m/s and  $R_{h(5 \text{ min})} = 0.868$  mm as intermediate results. This pressure differential is consistent with the higher probability of experiencing extreme combinations of wind and rainfall at this location compared to Pontevedra or Málaga.

#### 4.3. Comparison of Results Using the Original BPB Method and Limited Sub-Daily Data

If the previous results are compared with those obtained by neglecting the extrapolation between the duration of the tests and the available recording interval (i.e., without using Equations (6) and (8)), significant errors are observed in the characterization of watertightness performance and the pressure differential to be withstood (Table 4). These errors consistently cause unsecure designs by quantifying watertightness performances that are higher than the actual facade capabilities and reducing the pressure differentials to surpass during watertightness tests. These errors are smaller when the available recording interval is close to the duration of the test (see the case of Pontevedra, which has 10 min available records).

**Table 4.** Comparison with the results obtained by neglecting the use of proposed Equations (6) and (8).

<b>Málaga</b>			
	Using Equations (6) and (8)	Without using Equations (6) and (8)	Error
Case A (years)	78.3	482.4	+516.1%
Case B (Pa)	446	248	−44.4%
<b>Pontevedra</b>			
	Using Equations (6) and (8)	Without using Equations (6) and (8)	Error
Case A (years)	108.5	108.5 *	-
Case B (Pa)	329	309	−6.8%
<b>San Javier</b>			
	Using Equations (6) and (8)	Without using Equations (6) and (8)	Error
Case A (years)	11.1	33.9	+205.4%
Case B (Pa)	1102	528	−52.1%

\* In this case, the duration of the test matches the available recording interval at the location. Consequently, the result is not affected by the omission of Equations (6) and (8).

In addition, the comprehensive implementation of the BPB method in Spain can be achieved without the need to generate climatic data associated with numerous recording intervals, as was performed in the analyzed case studies. For instance, only daily data series can be aggregated to the available records at each location (i.e., 10, 30, and 60 min records by region). The average values of the annual maxima for each variable corresponding to both

recording intervals are provided in Table 3. By applying the LSR analysis to each pair of values, alternative coefficients  $a$ ,  $b$ ,  $c_{SIM}$ , and  $d_{SIM}$  can be determined for use in Equations (6) and (8), without generating additional series for other recording intervals (Table 5).

**Table 5.** Comparison with the results obtained by aggregating only a daily data series at each location.

<b>Málaga</b>				<b>Limited Equation (6) (by LSR)</b>	<b>Limited Equation (8) (by LSR)</b>
	Using all the aggregate series	Using 30 min and daily series	Error	$R_h(t) = 8.019 \cdot t^{-0.727}$	$U_{10SIM(t)} = -1.094 \cdot \ln(t) + 8.991$
Case A (years)	78.3	83.8	+7.0%		
Case B (Pa)	446	434	−2.7%		
<b>Pontevedra</b>				<b>Limited Equation (6) (by LSR)</b>	<b>Limited Equation (8) (by LSR)</b>
	Using all the aggregate series	Using 10 min and daily series	Error	$R_h(t) = 4.529 \cdot t^{-0.629}$	$U_{10SIM(t)} = -1.355 \cdot \ln(t) + 12.944$
Case A (years)	108.5	108.5 *	-		
Case B (Pa)	329	319	−3.0%		
<b>San Javier</b>				<b>Limited Equation (6) (by LSR)</b>	<b>Limited Equation (8) (by LSR)</b>
	Using all the aggregate series	Using hourly and daily series	Error	$R_h(t) = 9.306 \cdot t^{-0.724}$	$U_{10SIM(t)} = -1.062 \cdot \ln(t) + 9.527$
Case A (years)	11.1	10.4	−6.3%		
Case B (Pa)	1102	1159	+5.2%		

\* In this case, no data conversion between different time intervals is necessary, as the duration of the test matches the available recording interval at the location. Consequently, the result is not affected by the variation of the coefficients  $a$ ,  $b$ ,  $c_{SIM}$ , and  $d_{SIM}$ .

By repeating the calculations shown in Sections 4.1 and 4.2 using these alternative coefficients, it is observed that accuracy loss does not exceed 10% in any of the locations and case studies. These results confirm the feasibility of applying the proposed methodological refinements throughout Spain with a reduced computational effort. Furthermore, the BPB method can be applied based on any single series of sub-daily climatic records (with additional series for the other recording interval generated from the initial one): the results show no appreciable difference in accuracy when using data with 10, 30, or 60 min resolution as a starting point in conjunction with daily data.

In any case, the re-analysis and intermediate cross-multiplication conducted (even when limited sub-daily data are considered) result in a significant accuracy increase compared to relying on unscreened wind speed records, both concurrent and non-concurrent with rainfall. Thus, if the  $c$  and  $d$  coefficients tabulated in Table 3, along with the  $\mu_{(U_{10})}$  and  $\beta_{(U_{10})}$  parameters corresponding to all available wind speed records, are used in the calculation, the errors in characterizing watertightness performance can exceed 40% (as shown in Table 6).

As demonstrated through these case studies, the database presented in the Supplementary Material provides a reliable and accurate tool for quantitatively estimating the facade watertightness performance even in Spanish locations lacking exhaustive climatic records, due to the methodological refinements that enhance both the practicality and reliability of the BPB method:

- Maintaining the physical sense of the equation system to achieve greater reliability, using only calculation parameters related to wind speed values concurrent with rainfall (i.e., those actually affecting rainwater penetration into building facades).
- Enabling the application of the BPB method with any sub-daily climatic series, allowing for accurate estimations of watertightness performance regardless of the exhaustiveness of this available recording interval. This reduces reliance on exhaustive and costly raw climatic databases and significantly decreases the computational effort required to expand the current database with additional locations in Spain.



**Table 6.** Comparison with the results obtained by considering unscreened wind speed records.

<b>Málaga</b>			
	Using wind speed records concurrent with rainfall	Using unscreened wind speed records	Error
<i>Case A (years)</i>	78.3	47.1	−39.8%
<i>Case B (Pa)</i>	446	457	+2.5%
<b>Pontevedra</b>			
	Using wind speed records concurrent with rainfall	Using unscreened wind speed records	Error
<i>Case A (years)</i>	108.5	63.0	−41.9%
<i>Case B (Pa)</i>	329	367	+11.6%
<b>San Javier</b>			
	Using wind speed records concurrent with rainfall	Using unscreened wind speed records	Error
<i>Case A (years)</i>	11.1	12.7	+14.4%
<i>Case B (Pa)</i>	1102	885	−19.7%

Nevertheless, the implementation of the BPB method in Spain should be complemented with conservative safety factors, due to the stochastic nature of the analyzed variables (wind speed and rainfall intensity), the statistical nature of the return period (since there is no guarantee that exposure conditions linked to a specific return period will not occur more frequently), and the increasing unpredictability resulting from climate change. In this regard, it is recommended to extend the analyzed period whenever possible and to frequently update the data to reduce uncertainties. In turn, it may be advisable to assess how changing climate patterns could affect long-term facade performance, for instance, by generating weather variables for reference scenarios and climate change projections—an analysis that falls outside the scope of this article. Finally, the required watertightness performance should be critically assessed in each case based on design criteria, regulatory requirements, the public or private nature of the building, the expected service life of the facade, and other relevant factors.

## 5. Conclusions

In this study, the implementation of a quantitative and reliable approach for determining the watertightness performance of building facades under actual service conditions, as well as for estimating the required pressure differential to be withstood in any watertightness test to meet specific design requirements (BPB method), was addressed across 10 Spanish regions.

Through this implementation, specific methodological refinements that enhance the reliability and practicality of the BPB method were also addressed: (1) enhancing the physical consistency of the formulation by re-analyzing weather records to obtain the mode and dispersion parameters of wind speed maxima series concurrent with rainfall and (2) identifying general regressions that allow for the extrapolation of extreme values for rainfall and wind speed across any sub-daily time resolution, thereby eliminating the implementation requirement for weather data with exhaustive recording intervals.

Consequently, a comprehensive database is presented in the Supplementary Materials, summarizing the site-specific regressions and calculation parameters that enable the implementation of the BPB method at 360 Spanish locations. This database, which serves to support design decisions for preventing rainwater penetration in Spanish facades in a performance-based and practical manner, represents a significant starting point toward the automation of the method's equation-solving process. The same approach could also be applied in other regions and countries with available sub-daily weather data, provided that the correlations obtained through the proposed potential and logarithmic regressions (Equations (6)–(8)) are validated.

The use of this database in two case studies located in three Spanish locations representative of different climatic and facade operating conditions demonstrated that the increased mathematical consistency achieved through the proposed regressions allows for a significant reduction in calculation error (Table 4). Moreover, this accuracy was not significantly affected by the time resolution of the available sub-daily recording interval at the site, nor by using a single additional series of aggregate weather data (Table 5). Considering only those wind records concurrent with rainfall, thereby improving the physical relevance of the method's formulation, also provided a significant enhancement in calculation accuracy (Table 6).

**Supplementary Materials:** The following supporting information can be downloaded at <https://www.mdpi.com/article/10.3390/buildings14113542/s1>, Spreadsheet S1: Database for watertightness design of Spanish building facades using the refined BPB method.

**Author Contributions:** Conceptualization, J.M.P.-B. and J.D.-H.; data curation, Á.S.-B.; formal analysis, J.D.-H.; funding acquisition, J.M.P.-B.; investigation, J.M.P.-B.; methodology, M.O.-C.; project administration, J.M.P.-B.; resources, Á.S.-B.; software, M.O.-C.; supervision, S.A.O.; validation, Á.S.-B.; visualization, J.D.-H.; writing—original draft, J.M.P.-B.; writing—review and editing, J.D.-H. and S.A.O. All authors have read and agreed to the published version of the manuscript.

**Funding:** This research and the APC were funded by Project PID2021-122203OB-I00 funded by MCIN/AEI/10.13039/501100011033 and by ERDF A way of making Europe.

**Data Availability Statement:** The original contributions presented in the study are included in the article and Supplementary Materials, further inquiries can be directed to the corresponding author.

**Acknowledgments:** The results presented were partially obtained from data provided by the Agroclimatic Information System for Irrigation, Spanish Ministry of Agriculture, Fisheries, and Food. The authors acknowledge the help provided by engineers Elena Ibarz Montaner and Alicia C. Casas Aguirre with the data processing, as well as the collaboration of doctor in geological science Pedro L. López Julián.

**Conflicts of Interest:** The authors declare no conflicts of interest. The funders had no role in the design of the study; in the collection, analyses, or interpretation of data; in the writing of the manuscript; or in the decision to publish the results.

## Nomenclature

### Latin symbols

a, b, c, d	Site-dependent empirical coefficients (-)
$C_p$	Pressure coefficient (-)
P	Probability of occurrence
$R_h$	Rainfall record (mm or L/m <sup>2</sup> )
t	Recording interval (min)
$U_{10}$	Wind speed record (m/s)
z	Facade height (m)
$z_0$	Terrain roughness length (m)
$z_{data}$	Measurement height of wind speed (m)

### Greek symbols

$\Delta P$	Pressure differential (Pa)
$\beta_{(U_{10})}$	Dispersion of the annual maxima series of wind speed records (m/s)
$\beta_{(R_h)}$	Dispersion of the annual maxima series of rainfall records (mm or L/m <sup>2</sup> )
$\theta$	Angle between the wind direction and wall normal (°)
$\mu_{(U_{10})}$	Mode of the annual maxima series of wind speed records (m/s)
$\mu_{(R_h)}$	Mode of the annual maxima series of rainfall records (mm or L/m <sup>2</sup> )
$\varphi$	Density of the air (kg/m <sup>3</sup> )

### Subscripts

SIM	Relative to conditions concurrent with rainfall
t	Relative to the recording interval
z	Relative to the facade height

## References

1. Kubilay, A.; Bourcet, J.; Gravel, J.; Zhou, X.; Moore, T.V.; Lacasse, M.A.; Carmeliet, J.; Derome, D. Combined use of wind-driven rain load and potential evaporation to evaluate moisture damage risk: Case study on the parliament buildings in Ottawa, Canada. *Buildings* **2021**, *11*, 476. [\[CrossRef\]](#)
2. Wang, J.; Zhang, Y.; Li, B.; Zhao, Z.; Huang, C.; Zhang, X.; Deng, Q.; Lu, C.; Qian, H.; Yang, X.; et al. Effects of mold, water damage and window pane condensation on adult rhinitis and asthma partly mediated by different odors. *Build. Environ.* **2023**, *227*, 109814. [\[CrossRef\]](#)
3. Orr, S.A.; Cassar, M. Exposure indices of extreme wind-driven rain events for built heritage. *Atmosphere* **2020**, *11*, 163. [\[CrossRef\]](#)
4. Yu, S.; Liu, X.; Li, Y.; He, S.; Yao, Y.; Sun, S. Experimental and numerical simulation study on hygrothermal migration of damaged envelope walls during wind-driven rain. *Build. Environ.* **2023**, *243*, 110653. [\[CrossRef\]](#)
5. Hu, X.; Zhang, H.; Yu, H. Numerical simulation study on the hygrothermal performance of building exterior walls under dynamic wind-driven rain condition. *Build. Simul.* **2024**, *17*, 207–221. [\[CrossRef\]](#)
6. Wang, L.; Defo, M.; Xiao, Z.; Ge, H.; Lacasse, M.A. Stochastic simulation of mould growth performance of wood-frame building envelopes under climate change: Risk assessment and error estimation. *Buildings* **2021**, *11*, 333. [\[CrossRef\]](#)
7. Blocken, B.; Carmeliet, J. A review of wind-driven rain research in building science. *J. Wind. Eng. Ind. Aerodyn.* **2004**, *92*, 1079–1130. [\[CrossRef\]](#)
8. Cornick, S.M.; Lacasse, M.A. A review of climate loads relevant to assessing the watertightness performance of walls, windows and wall-window interfaces. *J. ASTM Int.* **2005**, *2*, 1–15. [\[CrossRef\]](#)
9. Blocken, B.; Derome, D.; Carmeliet, J. Rainwater runoff from building facades: A review. *Build. Environ.* **2013**, *60*, 339–361. [\[CrossRef\]](#)
10. Van Linden, S.; Van den Bossche, N. Review of rainwater infiltration rates in wall assemblies. *Build. Environ.* **2022**, *219*, 109213. [\[CrossRef\]](#)
11. Støver, E.A.; Sundsøy, M.H.; Andenæs, E.; Geving, S.; Kvande, T. Rain intrusion through horizontal joints in facade panel systems—Experimental investigation. *Buildings* **2022**, *12*, 1497. [\[CrossRef\]](#)
12. Lacy, R.E.; Shellard, H.C. An index of driving rain. *Meteorol. Mag.* **1962**, *91*, 177–184.
13. Qian, T.; Zhang, H. Assessment of long-term and extreme exposure to wind-driven rain for buildings in various regions of China. *Build. Environ.* **2021**, *189*, 107524. [\[CrossRef\]](#)
14. Giarma, C.; Aravantinos, D. On building components' exposure to driving rain in Greece. *J. Wind. Eng. Ind. Aerodyn.* **2014**, *125*, 133–145. [\[CrossRef\]](#)
15. Narula, P.; Sarkar, K.; Azad, S. Indexing of driving rain exposure in India based on daily gridded data. *J. Wind. Eng. Ind. Aerodyn.* **2018**, *175*, 244–251. [\[CrossRef\]](#)
16. Xiao, Z.; Lacasse, M.A.; Dragomirescu, E.; Defo, M. Projected changes of wind-driven rain and moisture load in wall assemblies across Canada. *J. Wind. Eng. Ind. Aerodyn.* **2023**, *238*, 105446. [\[CrossRef\]](#)
17. Orr, S.A.; Viles, H. Characterisation of building exposure to wind-driven rain in the UK and evaluation of current standards. *J. Wind. Eng. Ind. Aerodyn.* **2018**, *180*, 88–97. [\[CrossRef\]](#)
18. Pérez-Bella, J.M.; Domínguez-Hernández, J.; del Coz-Díaz, J.J.; Martínez-Martínez, J.E. Directional characterisation of annual and temporary exposure to rainwater penetration on building facades throughout Mexico. *Build. Environ.* **2022**, *212*, 108837. [\[CrossRef\]](#)
19. Domínguez-Hernández, J.M.; Pérez-Bella, J.; Alonso-Martínez, M.; Cano-Suñén, E.; del Coz-Díaz, J.J. Assessment of water penetration risk in building facades throughout Brazil. *Build. Res. Inf.* **2017**, *45*, 492–507. [\[CrossRef\]](#)
20. Blocken, B.; Stathopoulos, T.; Carmeliet, J.; Hensen, J.L.M. Application of computational fluid dynamics in building performance simulation for the outdoor environment: An overview. *J. Build. Perform. Simul.* **2011**, *4*, 157–184. [\[CrossRef\]](#)
21. Bai, X.; Gao, Y.; Di, Y.; Guan, J.; Jiang, L.; Fan, Z.; Hu, G. Analysis of numerical simulations and semi-empirical models on distribution characteristics of wind-driven rain on low-rise building facades. *Build. Environ.* **2024**, *263*, 111904. [\[CrossRef\]](#)
22. CEN EN ISO 12865; Hygrothermal Performance of Building Components and Building Elements—Determination of the Resistance of External Wall Systems to Driving Rain Under Pulsating Air Pressure. European Committee for Standardization: Brussels, Belgium, 2001.
23. CEN EN 12155; Curtain Walling—Watertightness—Laboratory Test Under Static Pressure. European Committee for Standardization: Brussels, Belgium, 2000.
24. AS/NZS 4284; Testing of Building Facades. Australian/New Zealand Standards: Sydney, Australia; Wellington, New Zealand, 2008.
25. ASTM E514; Standard Test Method for Water Penetration and Leakage Through Masonry. American Society for Testing and Materials: West Conshohocken, PA, USA, 2020. [\[CrossRef\]](#)
26. ASTM E547; Standard Test Method for Water Penetration of Exterior Windows, Skylights, Doors, and Curtain Walls by Cyclic Static Air Pressure Difference. American Society for Testing and Materials: West Conshohocken, PA, USA, 2016. [\[CrossRef\]](#)
27. SS 654:2020; Code of Practice for Curtain Walls. Enterprise Singapore: Singapore, 2020.
28. Choi, E.C.C. Criteria for water penetration testing. In *Water Leakage Through Building Facades*; ASTM STP 1314; Kudder, R.J., Erdly, J.L., Eds.; American Society for Testing and Materials: West Conshohocken, PA, USA, 1998; pp. 3–16.

29. Sahal, N.; Lacasse, M.A. Proposed method for calculating water penetration test parameters of wall assemblies as applied to Istanbul, Turkey. *Build. Environ.* **2008**, *43*, 1250–1260. [[CrossRef](#)]
30. Van den Bossche, N.; Lacasse, M.A.; Janssens, A. A uniform methodology to establish test parameters for watertightness testing Part II: Pareto front analysis on co-occurring rain and wind. *Build. Environ.* **2013**, *63*, 157–167. [[CrossRef](#)]
31. Pérez, J.M.; Domínguez, J.; Rodríguez, B.; del Coz, J.J.; Cano, E. A new method for determining the water tightness of building facades. *Build. Res. Inf.* **2013**, *41*, 401–414. [[CrossRef](#)]
32. Pérez-Bella, J.M.; Domínguez-Hernández, J.; Rodríguez-Soria, B.; del Coz-Díaz, J.J.; Cano-Suñén, E.; Navarro-Manso, A. An extended method for comparing watertightness tests for facades. *Build. Res. Inf.* **2013**, *41*, 706–721. [[CrossRef](#)]
33. Pérez, J.M.; Domínguez, J.; Rodríguez, B.; Cano, E.; del Coz, J.J.; Álvarez, F.P. Improvement alternatives for determining the watertightness performance of building facades. *Build. Res. Inf.* **2015**, *43*, 723–736. [[CrossRef](#)]
34. Pérez-Bella, J.M.; Domínguez-Hernández, J.; Cano-Suñén, E.; del Coz-Díaz, J.J.; Suárez-Domínguez, F.J. A comparison of methods for determining watertightness test parameters of building façades. *Build. Environ.* **2014**, *78*, 145–154. [[CrossRef](#)]
35. WMO. *Guide to Meteorological Instruments and Methods of Observation* (WMO No. 8); World Meteorological Organization: Geneva, Switzerland, 2008.
36. Jacobson, M.Z. *Fundamentals of Atmospheric Modelling*, 2nd ed.; Cambridge University Press: New York, NY, USA, 2005.
37. Smedman-Högström, A.S.; Högström, U. A practical method for determining wind frequency distributions for the lowest 200 m from routine meteorological data. *J. Appl. Meteorol.* **1978**, *17*, 942–954. [[CrossRef](#)]
38. Gualteri, G.; Secci, S. Comparing methods to calculate atmospheric stability-dependent wind speed profiles: A case study on coastal location. *Renew. Energy* **2011**, *36*, 2189–2204. [[CrossRef](#)]
39. Bañuelos-Ruedas, F.; Angeles-Camacho, C.; Rios-Marcuello, S. Analysis and validation of the methodology used in the extrapolation of wind speed data at different heights. *Renew. Sustain. Energy Rev.* **2010**, *14*, 2383–2391. [[CrossRef](#)]
40. Hoppestad, S. *Slagregninorge (Driving Rain in Norway, in Norwegian)*; NBI Report No. 13; Norwegian Building Research Institute: Oslo, Norway, 1955.
41. Lacy, R.E. Driving-rain maps and the onslaught of rain on buildings. In Proceedings of the RILEM/CIB Symposium on Moisture Problems in Buildings, Helsinki, Finland, 16–19 August 1965.
42. Straube, J.F.; Burnett, E.F.P. Simplified prediction of driving rain on buildings. In Proceedings of the International Building Physics Conference, Eindhoven, The Netherlands, 18–21 September 2000; pp. 375–382.
43. Van der Bossche, N.; Lacasse, M.A.; Janssens, A. A uniform methodology to establish test parameters for watertightness testing: Part I: A critical review. *Build. Environ.* **2013**, *63*, 145–156. [[CrossRef](#)]
44. Cornick, S.M.; Dalglish, A.; Said, N.; Djebbar, R.; Tariku, F.; Kumaran, M.K. *Report from Task 4 of MEWS Project: Task 4—Environmental Conditions Final Report (Research Report No. 113)*; National Research Council Canada: Ottawa, ON, Canada, 2002.
45. Gumbel, E.J. *Statistics of Extremes*; Columbia University Press: New York, NY, USA, 1958.
46. Pérez, J.M.; Domínguez, J.; Orr, S.A.; Sanso, L.; Ayensa, A. A comprehensive approach to the performance-based design of facade solutions against rainwater penetration. In Proceedings of the 10th Euro-American Congress of Construction Pathology, Rehabilitation Technology and Heritage Management (REHABEND 2024), Gijón, Spain, 7–10 May 2024; pp. 398–406.
47. Pérez-Bella, J.M.; Domínguez-Hernández, J.; Martínez-Martínez, J.E.; Alonso-Martínez, M.; del Coz-Díaz, J.J. An alternative approach to estimate any subdaily extreme of rainfall and wind from usually available records. *Stoch. Environ. Res. Risk Assess.* **2022**, *36*, 1819–1833. [[CrossRef](#)]
48. Tellinghuisen, J. Least-squares analysis of data with uncertainty in y and x: Algorithms in Excel and KaleidaGraph. *J. Chem. Educ.* **2018**, *95*, 970–977. [[CrossRef](#)]
49. Hersbach, H.; Bell, H.; Berrisford, P.; Biavati, G.; Horányi, A.; Muñoz-Sabater, J.; Nicolas, J.; Peubey, C.; Radu, R.; Rozum, I.; et al. ERA5 hourly data on single levels from 1940 to present. In *Copernicus Climate Change Service (C3S)—Climate Data Store (CDS)*; Copernicus Climate Change Service (C3S): Brussels, Belgium, 2023. [[CrossRef](#)]
50. Peel, M.C.; Finlayson, B.L.; McMahon, T.A. Updated world map of the Köppen-Geiger climate classification. *Hydrol. Earth Syst. Sci.* **2007**, *11*, 1633–1644. [[CrossRef](#)]
51. Atlas Nacional de España (ANE). Mapa de Clasificación Climática Según Köppen. 1981–2010 (CC BY 4.0 ign.es, Participantes y Fuentes de Datos). Available online: [https://educativo.ign.es/atlas-didactico/clima-eso/el\\_clima\\_en\\_espaa.html](https://educativo.ign.es/atlas-didactico/clima-eso/el_clima_en_espaa.html) (accessed on 11 September 2024).
52. Xunta of Galicia. Observation. Weather Reports. Data Access. Station List. Available online: <https://www.meteogalicia.gal/observacion/rede/redeIndex.action> (accessed on 11 September 2024).
53. Junta of Andalusia. Andalusian Agro-Climatic Information Network. Available online: <https://www.juntadeandalucia.es/agriculturaypesca/ifapa/riaweb/web/estacion/29/1> (accessed on 11 September 2024).
54. Government of the Basque Country. Department of Food, Rural Development, Agriculture and Fisheries. Weather Data. Available online: [https://www.euskadi.eus/web01-a3estand/es/?r01kSrchSrcId=contenidos.inter&r01kTgtPg=2&r01kLang=es&r01kQry=tC%3Aeuskadi%3BtF%3Aopendata%3Bt%3Aads\\_meteorologicos%3Bm%3AdocumentName.LIKE.lecturas%2CdocumentLanguage.EQ.es%3Bp%3Ainter%3Bpp%3Ar01PageSize.10&r01kPgCmd=2#contenidos.inter](https://www.euskadi.eus/web01-a3estand/es/?r01kSrchSrcId=contenidos.inter&r01kTgtPg=2&r01kLang=es&r01kQry=tC%3Aeuskadi%3BtF%3Aopendata%3Bt%3Aads_meteorologicos%3Bm%3AdocumentName.LIKE.lecturas%2CdocumentLanguage.EQ.es%3Bp%3Ainter%3Bpp%3Ar01PageSize.10&r01kPgCmd=2#contenidos.inter) (accessed on 11 September 2024).



55. Government of La Rioja. Agro-Climatic Information. Personalized Request. Available online: <https://www.larioja.org/agricultura/es/informacion-agroclimatica/red-estaciones-agroclimaticas-siar/consulta-personalizada> (accessed on 11 September 2024).
56. Agrarian Technological Institute of Castile and León. Weather Data from InfoRiego Network. Available online: [https://ftp.itacyl.es/Meteorologia/Datos\\_observacion\\_Red\\_InfoRiego/](https://ftp.itacyl.es/Meteorologia/Datos_observacion_Red_InfoRiego/) (accessed on 11 September 2024).
57. Spanish Ministry of Agriculture, Fisheries and Food. Agro-Climatic Information System for Irrigation. Available online: <https://servicio.mapa.gob.es/websiar/SeleccionParametrosMap.aspx?dst=1> (accessed on 11 September 2024).
58. Spanish Ministry of Agriculture, Fisheries and Food. Links of Interest: Irrigation Advisory Centres of the SiAR Network. Available online: <https://www.mapa.gob.es/es/desarrollo-rural/temas/gestion-sostenible-regadios/sistema-informacion-agroclimatica-regadio/informaciondeinteres.aspx> (accessed on 11 September 2024).
59. Diez, J.J.; Esteban, M.D.; López-Gutiérrez, J.S.; Negro, V. Meteocean influence on inland and coastal floods in the east of Spain. *J. Coast. Res.* **2013**, *29*, 72–80. [[CrossRef](#)]

**Disclaimer/Publisher’s Note:** The statements, opinions and data contained in all publications are solely those of the individual author(s) and contributor(s) and not of MDPI and/or the editor(s). MDPI and/or the editor(s) disclaim responsibility for any injury to people or property resulting from any ideas, methods, instructions or products referred to in the content.